



Study of Conjugate Heat Transfer from Heated Plate by Turbulent Offset Jet in Presence of Freestream Motion using Low-Reynolds Number Modeling

S. Kumar Rathore

Department of Mechanical Engineering, National Institute of Technology Rourkela, Rourkela, Odisha, 769008, India

†Corresponding Author Email: isushilrathore@gmail.com

(Received March 12, 2018; accepted September 4, 2018)

ABSTRACT

The present study deals with conjugate heat transfer from a heated flat plate by a turbulent offset jet in presence of freestream motion. The turbulent convection in fluid and conduction in solid is solved in a coupled manner by simultaneously satisfying the equality of temperature and heat flux at the solid-fluid interface. The computations have been carried out using low-Reynolds number (LRN) $k-\omega$ SST model in the fluid region. The capability of LRN modeling have enabled to solve the entire boundary layer including the thin viscous sublayer due to which Moffatt vortices (secondary recirculation regions) have been captured near the corner of the wall where the turbulence Reynolds number is low. The bottom surface of solid plate is maintained at a constant temperature higher than the jet inlet temperature whereas the jet inlet temperature is same as that of the ambient. The present investigation reports the effects of offset ratio of jet (OR), Reynolds number of flow (Re), solid to fluid thermal conductivity ratio (K), solid slab thickness (S) and freestream velocity (U_∞) on conjugate heat transfer arises due to solid and fluid interaction. The offset ratio is varied in the range $OR = 3 - 11$, Reynolds number in the range $Re = 10000 - 25000$, solid to fluid thermal conductivity ratio in the range $K = 1 - 2000$, solid slab thickness in the range $S = 1-20$ and freestream velocity in the range $U_\infty = 0.1 - 0.25$. The effects of various parameters on the near-wall velocity profile, solid-fluid interface temperature, local Nusselt number variation along the plate, heat flux variation along the plate, etc. have been discussed in detail.

Keywords: Conjugate heat transfer; Offset jet; Low-Reynolds number model; Freestream motion; Numerical simulation.

NOMENCLATURE

G	production of turbulent kinetic energy by shear	T_{in}	jet inlet temperature
h	width of the nozzle	\bar{u}, \bar{v}	dimensional mean velocities in x, y - directions respectively
K	solid to fluid thermal conductivity ratio	U, V	non-dimensional velocities in X, Y - directions respectively
k_s, k_f	thermal conductivity of solid and fluid, respectively	u^+	non-dimensional velocity
\bar{p}_0	ambient pressure	U_0	average inlet jet velocity
\bar{p}	static pressure	U_∞	non-dimensional freestream velocity
P	non-dimensional static pressure	u_∞	freestream velocity
Pr	Prandtl number	u_τ	friction velocity
Pr_t	turbulent Prandtl number	X, Y	non-dimensional coordinates
Re	Reynolds number	x, y	dimensional coordinates
Re_t	turbulent Reynolds number	x^+	non-dimensional distance
S	non-dimensional thickness of solid flat plate	y^+	non-dimensional distance
s	thickness of solid flat plate	α, α_t	laminar and turbulent thermal diffusivities, respectively
T	dimensional temperature	ν, ν_t	laminar and turbulent kinematic viscosities, respectively
T_b	temperature at the bottom surface of plate		

ω rate of specific dissipation
 θ non-dimensional temperature

fluid condition
 n non-dimensional quantity
 p corresponds to the first near-wall grid point
 w corresponds to wall

Subscripts

∞ corresponds to freestream/surrounding

1. INTRODUCTION

The conjugate cooling of a solid flat plate by a turbulent offset jet is a important problem owing to many engineering applications such as cooling of hot metal slab, continuous casting, hot rolling and extrusion, cooling of turbine blades and combustion chamber walls, cooling of electronic equipments, etc. Turbulent jets are used in a variety of engineering applications for cooling, drying, defrosting of automobile windshield, airfoil boundary layer separation control, distribution of conditioned air in enclosed environment, discharge of effluent jet coming from waste water outlets, etc. (Lauder and Rodi 1981; Pelfrey and Liburdy 1986; Gao and Ewing 2007; Kumar and Das 2011; Rathore and Das 2016). The conjugate heat transfer problem arises in a situation when convection heat transfer in a fluid is affected by conduction in solid. Thus, convection in fluid and conduction in solid are required to be solved simultaneously as it is a coupled problem. Often, the thickness of solid body is assumed negligible and only the convection in the fluid domain is solved with idealized boundary condition on the solid surface. However, more realistic solution can be obtained by taking into account thickness along with thermo-physical properties of solid. The two boundary conditions are required to be satisfied for such coupled conjugate heat transfer problems: temperature at the solid-fluid interface should be equal i.e. $(\theta_i)_f = (\theta_i)_s$ and the heat flux at the solid-fluid interface should be equal i.e. $(q_{i,n})_f = (q_{i,n})_s$.

In offset jet case, the jet comes out from a nozzle certain height above the solid surface. The schematic diagram of turbulent offset jet in a presence of freestream motion is shown in Fig. 1. The ratio of distance between the jet center line and horizontal flat plate (H), and nozzle width (h) is known as offset ratio ($OR = H/h$). The flow immediately downstream of the nozzle exit consists of a potential core region where the flow remains unaffected from effects of viscosity and velocity is equal to the jet inlet velocity. In other words, centerline velocity remains constant without any decay in the potential core region. The flow over the plate can be divided into three regions namely the recirculation region, the impingement region and the wall jet region. The offset jet deflects towards the solid wall due to asymmetric entrainment above and below the jet and finally attaches with the solid plate at the reattachment point. This phenomenon is also known as Coanda effect (Tritton 1977) where the jet have the tendency to attach with the neighboring solid surface. The reattachment point is a location at which wall shear changes its direction

thus wall shear stress becomes zero at the reattachment point. The jet attaches with the solid plate in the impingement region. A part of fluid flows back into the recirculation region due to adverse pressure gradient prevailing in the recirculation region and the remaining fluid flow in the downstream direction. In the impingement region, flow stabilizes and interconversion of pressure and velocity takes place. After certain downstream distance, the flow acquires the characteristics of a generic wall jet flow thus known as wall jet region.

The experimental and theoretical study of flow field of turbulent offset jets in the presence of an external moving stream has been reported by Hoch and Jiji (1981a) for Reynolds number of 16000, offset ratios up to 8.7 and non-dimensional freestream velocity $U_\infty < 0.3$. The theoretical study has taken into account both variation in pressure and radius of curvature in the recirculation region. They have observed a good agreement between experimental and theoretical results. The same authors (Hoch and Jiji 1981) later on extended the work to study the heat transfer characteristics of turbulent offset jet for the same geometry. They have provided the experimental and analytical solutions for decay of the local maximum axial temperature. The experimental investigation of flow and heat transfer characteristics of turbulent offset jet has been reported by Kim *et al.* (1996) for offset ratios in the range 0 – 20 and Reynolds number in the range 6500 – 39000. They have carried out measurements of the mean velocity and turbulent intensity, and wall temperature using split film probe and thermochronic liquid crystal, respectively. They have reported that the point of maximum Nusselt number coincides with the time averaged reattachment point. They have also found the presence of a secondary vortex which causes better mixing and increases the Nusselt number near the corner. Recently, Habli *et al.* (2014) have reported the computational study of a turbulent plane jet flow in the presence of coflow motion using standard $k-\epsilon$ model. They have considered coflow velocity ratio up to 0.1. They have compared some of their computational results with the experimental results of Deo *et al.* (2007). They have concluded that velocity decay rate is lower for higher values of coflow velocity ratio and also reported that parameters can reach an asymptotic curve at different coflow velocity ratios when using a momentum length scale. In an another study, the mean flow and thermal characteristics of plane turbulent wall jet discharged into coflow stream is reported by Ayeche *et al.* (2017). The effect of deviation of coflow stream on the characteristics of the wall jet as compared with a wall jet in non-directed coflow is reported. For same velocity ratio,

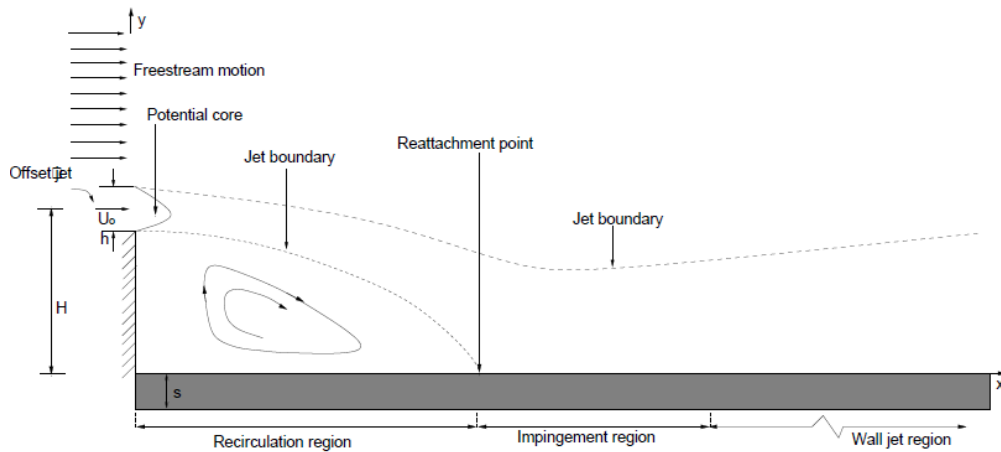


Fig. 1. Schematic diagram of conjugate cooling of solid plate of finite thickness by offset jet.

the increase in deviation angles of the coflow causes a rapid decrease of the longitudinal maximum velocity and a slight increase in the longitudinal maximum temperature. They have also noticed that both decay rate of the maximum velocity and spread rate of the jet increase with increase in coflow deviation.

The application of LRN turbulence models to numerically predict the flow and thermal characteristics of turbulent wall jet flow is first reported by [Kechiche *et al.* \(2004\)](#). They have considered Reynolds number in the range 7300 – 22500. The isothermal jet is submitted to the impingement wall which is maintained at either isothermal or constant heat flux boundary condition. Low-Reynolds number $k-\varepsilon$ models proposed by [Chien \(1982\)](#), [Nagano and Hishida \(1987\)](#) and [Herrero *et al.* \(1991\)](#) are considered for numerical simulations. The computed results are compared with experimental results available in the literature. They have found that for the case of non-isothermal wall jet, [Herrero *et al.* \(1991\)](#) model is more effective for predicting the thermal characteristics. [Rathore and Das \(2015\)](#) have carried out a comparative study of flow and heat transfer characteristics of turbulent offset jet and wall jet using standard $k-\varepsilon$ model, low-Reynolds number turbulence models proposed by [Launder and Sharma \(1974\)](#), [Yang and Shih \(1993\)](#), and $k-\omega$ SST model ([Menter 2009](#)). The results obtained from simulation have been compared with available experimental results. The capability of LRN models to resolve the entire boundary layer have enabled them to capture temperature profile in the thermal sublayer. Based on the comparison with experimental results, it has been found that LRN turbulence model proposed by [Yang and Shih \(1993\)](#) and $k-\omega$ SST model perform better.

[Vishnuvardhanarao and Das \(2007\)](#) have reported the conjugated heat transfer from a solid slab subjected to constant heat flux boundary condition by turbulent plane offset jet for $Re = 15000$. High-Reynolds-number (HRN) standard $k-\varepsilon$ model in conjunction with wall functions has been applied

for turbulence modeling. The effect of thermal conductivity ratio of solid and fluid, thickness of the solid slab and Prandtl number of the fluid on heat transfer characteristics has been investigated. The same authors ([Vishnuvardhanarao and Das 2009](#)) later on reported the study on solid slab subjected to constant isothermal temperature at the bottom. The isothermal temperature maintained at the bottom of the solid slab is higher than the offset jet inlet temperature. The conjugate heat transfer study from combined wall jet and offset jet flow is computationally investigated by [Mondal *et al.* \(2016\)](#) using standard $k-\varepsilon$ model in conjunction with wall functions. The ratio of distance between the two jets to the jet width is taken as one and the bottom wall of the solid slab is maintained at a constant temperature. They have varied Reynolds number (Re) in the range 10,000 and 20,000, Prandtl number (Pr) in the range 1 and 4, thermal conductivity ratio of solid and fluid in the range 1000 and 4000, and non-dimensional solid slab thickness in the range of 1–10. They have observed flow pattern near the nozzle exit similar to periodic vortex shedding as occurs in the case of flow past a two-dimensional bluff body. The interface temperature and local heat flux along the interface have been found to depend on Re , Pr , K and S .

In the present investigation, the conjugate cooling of solid flat plate by turbulent offset jet is considered in the presence of freestream motion. The bottom surface of flat plate is subjected to isothermal temperature whereas the inlet temperature of the offset jet is same as that of the ambient. The temperature of jet at the inlet and freestream temperature is same as that of ambient temperature. The solution have been obtained by tackling the turbulent convection in fluid and the conduction in the solid in a coupled manner. The effects of offset ratio of jet (OR), Reynolds number of flow (Re), solid to fluid thermal conductivity ratio (K), non-dimensional solid slab thickness (S) and freestream velocity (U_∞) on conjugate heat transfer characteristics have been investigated. The parameters are varied in the range $OR = 3 - 11$, $Re = 10000 - 25000$, $K = 1 - 2000$, $S = 1 - 20$ and U_∞

= 0.1 – 0.25. The turbulence closure has been obtained by using low-Reynolds number (LRN) $k - \omega$ SST model. The near-wall treatment in turbulent flow is very crucial to obtain the accurate results. The entire boundary layer including the thin viscous sublayer is resolved using very fine grids in the near-wall region. The advantage of LRN modeling is that no wall functions are required unlike high Reynolds modeling. Low-Reynolds number modeling is more appropriate for the present investigation as it involves separation region and also to capture secondary recirculation regions near the corner of the wall which otherwise can not be captured with high Reynolds number turbulence models. Based on the literature review, it has been observed that very few articles are available on conjugate cooling of flat plate in the presence of freestream motion using low-Reynolds number modeling. The present study is an attempt to bridge this gap in the literature.

2. MATHEMATICAL FORMULATION

2.1 Turbulence Model

$k - \omega$ SST model: It belongs to the family of two-equation, eddy viscosity based $k - \omega$ turbulence model. In the low-Reynolds number $k - \omega$ SST model, transport equations for turbulent kinetic energy and specific dissipation rate are solved up to the wall including the thin viscous sublayer region without using any extra damping function. The absence of extra damping function is one of the major advantage of this model as damping function induces stiffness during numerical solution. The $k - \omega$ SST model is obtained by blending the $k - \omega$ model in near-wall region and the $k - \varepsilon$ model away from wall. Thus, it combines the advantages of robust and accurate formulation of the $k - \omega$ model in the near-wall region and the freestream independence of $k - \varepsilon$ model away from the wall. In order to obtain the $k - \omega$ SST model, standard $k - \varepsilon$ model is first transformed into $k - \omega$ form. The resulting model in $k - \omega$ form is multiplied with $(1 - F_1)$ and the original model is multiplied with F_1 and then both are added together. The switching function F_1 is formulated in such a way that it takes a value of unity in near-wall region and $k - \omega$ model is activated. On the other hand, switching function F_1 assumes a value of zero for values of $y^+ > 70$ (Menter 1994) and the standard $k - \varepsilon$ model is activated in the outer region of boundary layer. The definition of turbulent eddy viscosity takes into account the transport of turbulent shear stress. These factors make the $k - \omega$ SST model suitable for wide range of flow problems including adverse pressure gradient flows, impingement type of flow, flow involving separation, localized laminar flow and transition in the flow, etc. Bardina *et al.* (1997) have considered 10 different forced convection flow cases of which 7 are relatively simple free-shear and zero-pressure-gradient boundary layer flows whereas the remaining 3 are complex flows involving separation. They have observed that $k - \omega$ SST model gives better agreement with the experimental results among the 4 models

considered. Similarly, Hofmann *et al.* (2007) have reported about the better performance of $k - \omega$ SST model for the steady and pulsating type impinging jet flows among the 13 popular and widely used turbulence models. Rathore and Das (2015) have also reported about the better performance of $k - \omega$ SST model for complex turbulent offset jet flow problem. The model constants of $k - \omega$ SST model are obtained by blending the corresponding constants of the $k - \omega$ and $k - \varepsilon$ models. Many modifications are incorporated into the original SST model in the last 15 years (Menter *et al.* 2003; Menter (2009)). For the present study, the $k - \omega$ SST model described in Menter [2009] is implemented.

2.2 Governing Equations

The Reynolds averaged Navier-Stokes (RANS) equations are used for predicting the turbulent flow. The mean flow is assumed to be steady and two-dimensional. The body forces are neglected and the fluid properties are assumed to be constant. The Boussinesq hypothesis is used to link the Reynolds stresses to the mean velocity gradients and turbulent eddy viscosity.

The dimensionless variables are defined as:

$$U_i = \frac{\bar{u}_i}{U_0}, \quad X_i = \frac{x_i}{h}, \quad \theta = \frac{T - T_\infty}{T_b - T_\infty} \quad (1)$$

$$P = \frac{\bar{p} - p_0}{\rho U_0^2}, \quad k_n = \frac{k}{U_0^2}, \quad \omega_n = \frac{\omega}{U_0/h}, \quad \nu_{t,n} = \frac{\nu_t}{\nu}$$

The non-dimensional equations are:

Continuity Equation:

$$\frac{\partial U_i}{\partial X_i} = 0 \quad (2)$$

Momentum equations:

$$U_j \frac{\partial U_i}{\partial X_j} = - \frac{\partial \left(P + \frac{2}{3} k_n \right)}{\partial X_i} + \frac{1}{\text{Re}} \frac{\partial}{\partial X_j} \left[(1 + \nu_{t,n}) \left(\frac{\partial U_i}{\partial X_j} + \frac{\partial U_j}{\partial X_i} \right) \right] \quad (3)$$

Turbulent kinetic energy (k_n) equation:

$$U_j \frac{\partial k_n}{\partial X_j} = \frac{1}{\text{Re}} \frac{\partial}{\partial X_j} \left[(1 + \sigma_k \nu_{t,n}) \frac{\partial k_n}{\partial X_j} \right] + \text{Min}(G_n, 10\beta^* k_n \omega_n) - \beta^* k_n \omega_n \quad (4)$$

Specific dissipation rate (ω_n) equation:

$$U_j \frac{\partial \omega_n}{\partial X_j} = \frac{1}{\text{Re}} \frac{\partial}{\partial X_j} \left[(1 + \sigma_\omega \nu_{t,n}) \frac{\partial \omega_n}{\partial X_j} \right] + \frac{\alpha \text{Re}}{\nu_{t,n}} \text{Min}(G_n, 10\beta^* k_n \omega_n) + \beta \omega_n^2 + 2(1 - F_1) \sigma_{\omega 2} \frac{1}{\omega_n} \frac{\partial k_n}{\partial X_j} \frac{\partial \omega_n}{\partial X_j} \quad (5)$$

The blending function F_1 given as

$$F_1 = \tanh \left[\left\{ \text{Min}(\zeta, \eta) \right\}^4 \right] \quad (6)$$

where

$$\zeta = \text{Max} \left(\frac{\sqrt{k_n}}{\beta^* \omega_n d}, \frac{500}{\text{Re} d^2 \omega_n} \right) \quad (7)$$

$$\eta = \frac{4\sigma_{\omega 2} \frac{k_n}{d^2}}{\text{Max} \left(2\sigma_{\omega 2} \frac{1}{\omega_n} \frac{\partial k_n}{\partial X_j} \frac{\partial \omega_n}{\partial X_j}, 10^{-10} \right)} \quad (8)$$

Eddy viscosity ($\nu_{t,n}$):

$$\nu_{t,n} = \text{Re} \text{Min} \left[\frac{k_n}{\omega_n}, \frac{a_1 k_n}{F_2 \sqrt{\frac{\partial U_i}{\partial X_j} \left(\frac{\partial U_i}{\partial X_j} + \frac{\partial U_j}{\partial X_i} \right)}} \right] \quad (9)$$

where

$$F_2 = \tanh \left[\left\{ \text{Max} \left(\frac{2\sqrt{k_n}}{\beta^* \omega_n d}, \frac{500}{\text{Re} d^2 \omega_n} \right) \right\}^2 \right] \quad (10)$$

Energy equation in the fluid region:

$$U_j \frac{\partial \theta}{\partial X_j} = \frac{1}{\text{Re} \cdot \text{Pr}} \frac{\partial}{\partial X_j} \left[(1 + \alpha_{t,n}) \frac{\partial \theta}{\partial X_j} \right] \quad (11)$$

Eddy diffusivity ($\alpha_{t,n}$) is given as:

$$\alpha_{t,n} = \frac{\text{Pr} \nu_{t,n}}{\text{Pr}_t} \quad (12)$$

Energy equation in the solid region:

$$\frac{\partial}{\partial x_j} \left(\frac{\partial \theta}{\partial x_j} \right) = 0 \quad (13)$$

The turbulent Prandtl number (Pr_t) is taken as equal to 0.9 for air (Biswas and Eswaran 2002).

The model constants are given as (Menter 2009):

$$\alpha_1 = 0.31, \beta^* = 0.09, \alpha_1 = 5/9, \alpha_2 = 0.44, \beta_1 = 0.075, \beta_1 = 0.0828, \sigma_{k1} = 0.85, \sigma_{k2} = 1.0, \sigma_{\omega 1} = 0.5, \sigma_{\omega 2} = 0.856,$$

$$\alpha = \alpha_1 F_1 + \alpha_2 (1 - F_1), \beta = \beta_1 F_1 + \beta_2 (1 - F_1), \sigma_k = \sigma_{k1} F_1 + \sigma_{k2} (1 - F_1), \alpha_{\omega} = \sigma_{\omega 1} F_1 + \sigma_{\omega 2} (1 - F_1)$$

2.3 Boundary conditions

The no-slip ($U = 0$) and no-penetration boundary conditions ($V = 0$) are imposed at the solid walls. The non-dimensional velocity components at the jet inlet are $U = 1$ and $V = 0$. The value of turbulent kinetic energy at the jet inlet and coflowing stream is $k_n = 1.5I^2$. In the present study, the turbulence intensity (I) at the jet inlet and coflowing stream is taken equal to 0.02 and 0.001, respectively. The rate

of specific dissipation (ω_n) at the jet inlet and the solid wall are prescribed as $\omega_n = k_n^{1/2} / (C_{\mu}^{1/4} 0.07)$

and $\omega_n = 60 / (Re \beta_1 \Delta Y_p^2)$ (Menter 1994)

respectively, where ΔY_p is the non-dimensional distance to the next near-wall grid point. The value of turbulent kinetic energy at the solid wall is taken as $k_n = 0$.

The temperature at the jet inlet and freestream are taken as $\theta = 0$. The temperature of vertical wall below the jet is considered as $\theta = 0$ and at the bottom of flat plate is maintained constant (isothermal) given as $\theta = 1$. The left and right end of the plate is adiabatic. The entrainment boundary conditions are $\theta = 0, \partial \phi / \partial Y = 0, k_n = 10^{-6}$ and $\omega_n = \lambda V_{\infty} / L$ where $\phi = U, V$. Here, L is the approximate non-dimensional length of the computational domain and λ is a constant. The value of λ is taken as 40 for mixing layer (Bardina *et al.* 1997). The developed condition of $\partial \phi / \partial n = 0$ ($\phi = U, V, k_n, \omega_n$ and θ) is imposed at the exit boundary. The two boundary conditions are required to be satisfied for conjugate heat transfer problem: temperature at the solid-liquid interface should be equal i.e. $(\theta_i)_f = (\theta_i)_s$ and the heat flux at the solid-liquid

interface should be equal i.e. $(q_{i,n})_f = (q_{i,n})_s$.

2.4 Near-wall treatment

The formation of viscous sublayer region is one of the distinguished characteristics of turbulent wall boundary layer. The transport of momentum and heat in this layer is mainly due to the viscous diffusion mechanism. The viscous diffusion mechanism becomes very strong for turbulent Reynolds number $\text{Re}_t < 100$ (Shuja *et al.* 1999) where turbulent Reynolds number $\text{Re}_t = k/\nu\omega$. Low-Reynolds number turbulence modeling employs very fine grid in the near-wall region to capture the entire boundary layer including the thin viscous sublayer region. The fine grid is required in the near-wall region in order to capture steep gradient of variables. Thus, no assumptions are required for mean velocity, temperature variation, etc. in the form of wall functions unlike the high-Reynolds number turbulence models. On the other hand, high-Reynolds number turbulence models do not solve the near-wall region instead the first near wall grid point is placed in the log-law layer with y^+ in the range 30-100. So basically, wall functions are used to bridge the inner region between the wall and the fully developed turbulence region. The more details about wall functions are given in Biswas and Eswaran (2002).

The wall functions are not applicable in many situations such as flow involving separation, localized laminar flow, transition, buoyant flow, etc. The proper near-wall treatment is essential for accurate solution procedure. However, the solution obtained using LRN model is computationally extensive due to very fine grids in the near-wall region as compared to the high Reynolds number turbulence model utilizing wall functions. The fine

grid in the near wall region also gives rise to numerical stiffness. To avoid these problems, proper source term linearization and proper grid density in the near wall region are essential for solution.

3. SOLUTION METHODOLOGY AND VALIDATION

The governing differential equations are solved in the non-dimensional form using in-house code in C++ language. The governing differential equations are discretized using the finite volume approach on a staggered grid. The power-law upwind and second-order central-difference schemes are used to discretize the convective and diffusive terms, respectively. The velocity-pressure coupling is done using SIMPLEC algorithm (Van Doormaal and Raithby 1984) which is extension of semi-implicit method for pressure-linked equation (SIMPLE) algorithm (Patankar 1980). The algebraic equations are solved using Tri-diagonal matrix algorithm (TDMA) and line-by-line solver. The TDMA traverse is employed in the cross-streamwise direction and a sweep from upstream to downstream is preferred to obtain a faster convergence. The under-relaxation of momentum, turbulent and energy equations have been done using the pseudo-transient approach as given in Versteeg and Malalasekera (1996). The fluid flow solution is obtained first and then it is utilized for solving energy equation as the flow is incompressible and the buoyancy effects are not present. In the present study, the thickness of solid plate is taken into account. Thus, conduction in the solid slab and convection in the fluid region are required to be solved simultaneously.

The non-dimensional domain size considered for the present study is 75×60 to solve the convective flow on the fluid side. For the grid independence study, effects of grid density and number of grids are tested. The grid independence study has been carried out with grid sizes 241×241 , 313×313 and 443×443 and the grid size of 241×241 is finally considered for the simulation in the fluid side. Non-uniform grid is considered with a staggered arrangement. The nonuniform grids have been drawn using the geometric expansion scheme $\Sigma = a(1 - r^n)/(1 - r)$, where a is the size of the first grid point, r is the expansion ratio and Σ is the domain size. Higher grid density is used near the wall and in the jet entrance region. The zoomed view of grid near the wall is shown in Fig. 2. It has been ensured that the first grid point near the wall lies in the viscous sublayer ($y^+ < 1.5$ and $x^+ < 1.0$). The variation of non-dimensional distance y^+ with axial distance X for the first near-wall grid point is shown in Fig. 3 for $OR = 7$ and $Re = 20000$. In order to validate the solution, the computational results obtained from $k - \omega$ SST model is compared with the experimental results of Pelfrey and Liburdy (1986) for offset ratio 7 and Reynolds number 15000 at various axial locations as shown in Fig. 4. All the axial locations viz. $X = 3, 6, 9, 12$ fall in the recirculation region. The negative value of velocity in the near-wall region is due to the presence of recirculation region. The local maximum axial velocity of jet decreases as flow proceeds in the downstream as

shown in Fig. 4. The more deviation is observed at $X = 12$ as this axial location is very close to the reattachment point where jet is subjected to stagnation. The flow near the stagnation point is very complex thus more deviations are observed at axial location $X = 12$. Overall, a good agreement has been observed despite some deviations between the computational and experimental results.

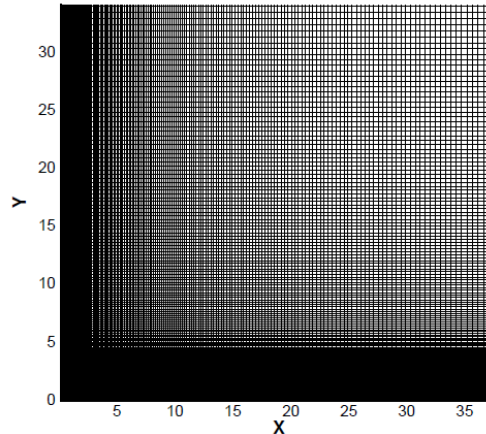


Fig. 2. Zoomed view of grid for $OR = 7$ and grid size 241×241 .

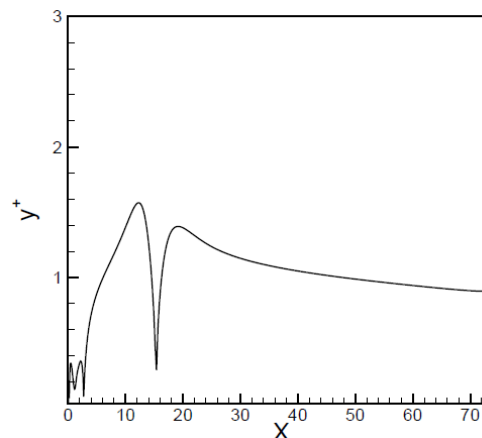


Fig. 3. Variation of y^+ with X for the first near-wall grid point for $OR = 7$ and $Re = 20000$.

4. RESULTS AND DISCUSSION

The computational study of conjugate heat transfer from offset jet flow has been carried out in the presence of freestream flow. The temperature of jet at the inlet and freestream temperature is same as that of the ambient. The bottom surface of the solid plate is maintained at hot uniform temperature. The effects of offset ratio of jet (OR), Reynolds number of flow (Re), solid to fluid thermal conductivity ratio (K), non-dimensional plate thickness (S) and freestream velocity (U_∞) on conjugate heat transfer characteristics have been considered. The offset ratio is varied in the range $OR = 3 - 11$, Reynolds number in the range $Re = 10000 - 25000$, thermal conductivity ratio in the range $K = 1 - 2000$, solid plate thickness $S = 1 - 20$ and freestream velocity in

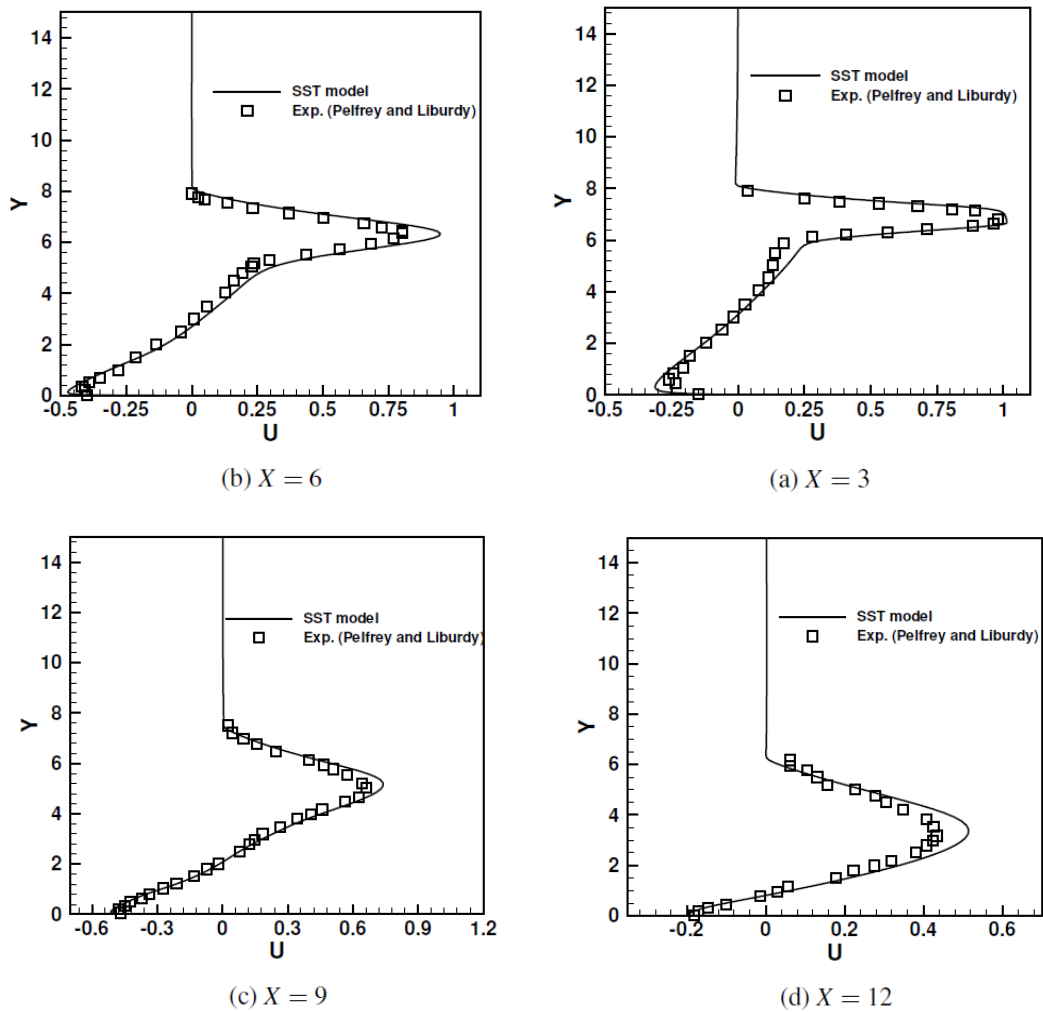


Fig. 4. Comparison of u velocity with experimental results of Pelfrey and Liburdy [1986] at various axial locations.

the range $U_\infty = 0.1 - 0.25$. The computations have been carried out using low-Reynolds number $k-\omega$ SST model. The entire boundary layer is solved including the very thin sublayer region using very fine grids in order to capture the sharp gradient of variables. The conduction in solid and convection in fluid are solved simultaneously to study the conjugate heat transfer characteristics.

Figure 5 shows the streamlines for various offset ratios for $Re=15000$ and $U_\infty = 0.20$. A recirculation region is formed near the jet inlet due to the presence of low-pressure region. The asymmetric rate of entrainment above and below the jet gives rise to the formation of low-pressure region. This phenomenon is also known as Coanda effect (Tritton 1977) as discussed earlier. The size of primary recirculation region increases with increase in offset ratio of jet. The streamlines above the jet are inclined which indicates the entrainment of surrounding freestream fluid into the jet. The zoomed view of streamlines are shown in Fig. 6. The presence of two secondary recirculation regions have been identified near the corner of the wall in addition to primary recirculation region. The flow

near corner of the wall is mainly dominated by the viscous diffusion mechanism due to low turbulence Reynolds number. Moffatt (1964) had shown that the flow near corner of the wall consists of a sequence of eddies of decreasing size and intensity. The near-wall region must be solved with very fine grids in order to capture the eddies near corner of the wall. In the present simulation, two closed series of secondary recirculation regions have been captured as the entire boundary layer is solved including the viscous sublayer with very fine grids. The size of secondary recirculation region increases with increase in offset ratio of jet.

Figure 7 shows the variation of velocity profile in non-dimensional coordinates ($u^+ - y^+$) for different values of freestream velocity in the similarity wall jet region at $X = 50$ where other parameters are set as $Re = 15000$ and $OR = 7$. The velocity profiles become nearly self-similar in similarity wall jet region. The law of the wall $u^+ = y^+$ and the universal log-law profile $u^+ = 2.44 \ln(y^+) + 5.0$ is also superimposed on the same plot. The effect of freestream motion is evident only in the outer region away from the wall. The velocity profile in the near-wall

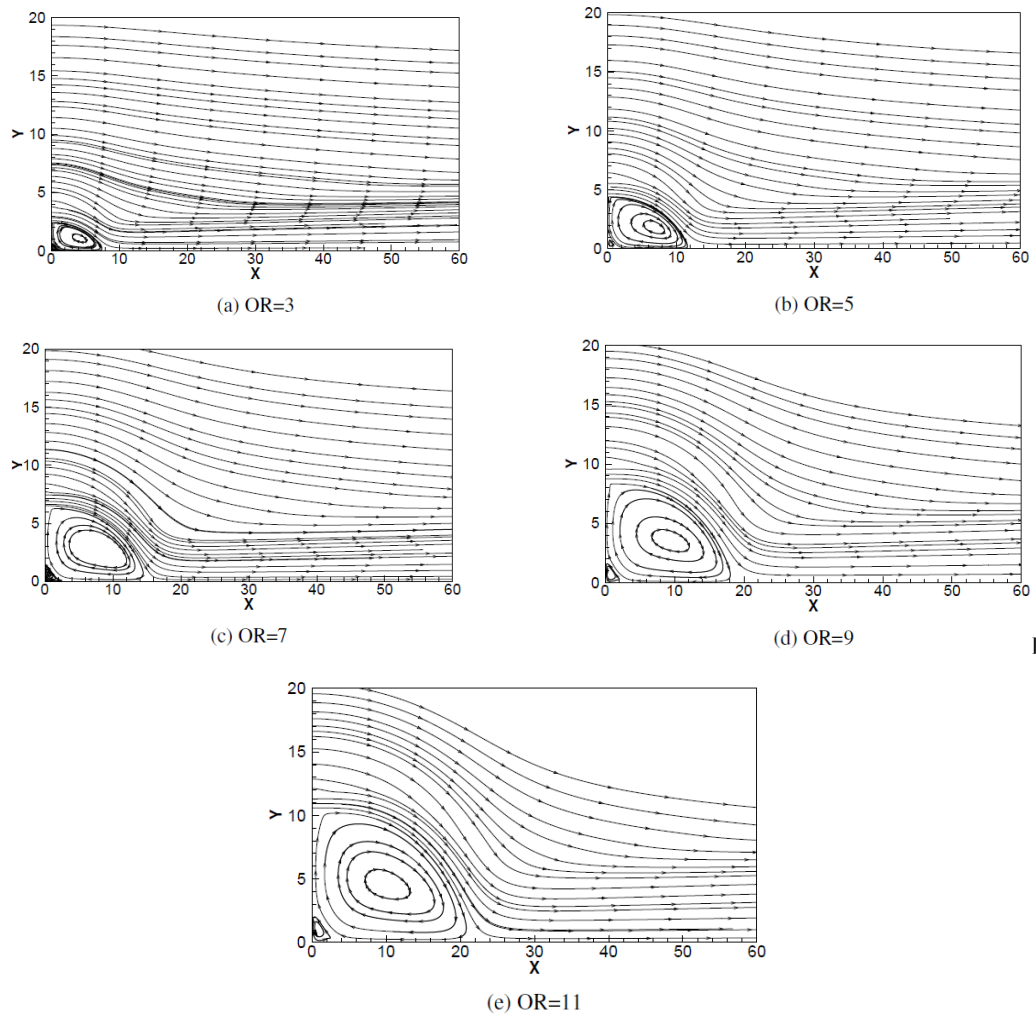


Fig. 5. Streamlines for $Re=15000$, $U_{inf} = 0.20$.

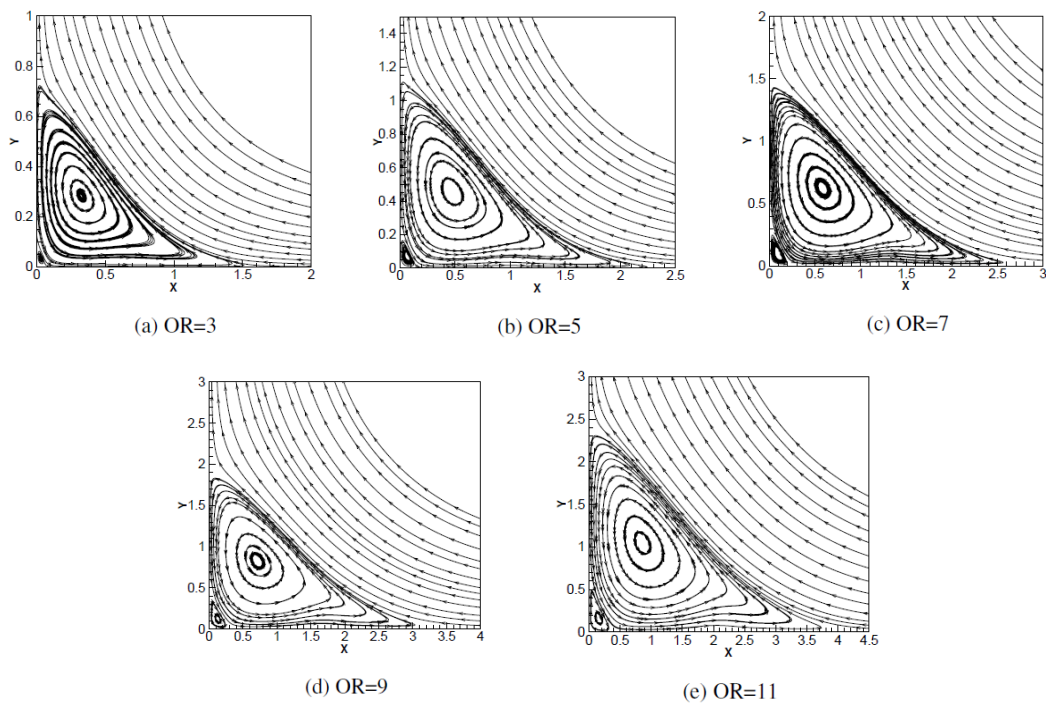


Fig. 6. Zoomed view of streamlines showing secondary vortices for $Re=15000$, $U_{inf} = 0.20$.

region does not show any variation for different values of freestream velocity. The effect of Reynolds number on the $u^+ - y^+$ profile at $X = 50$ is shown in Fig. 8 for $OR = 7$ and $U_\infty = 0.2$. The non-dimensional velocity in the outer layer is higher for higher Reynolds number whereas non-dimensional velocity profiles for different Reynolds number collapse on each other in the near-wall region. Figure 9 shows the variation of velocity profile in non-dimensional coordinates ($u^+ - y^+$) for different values of offset ratio in the similarity wall jet region ($X = 50$) for $Re = 15000$ and $OR = 7$. The non-dimensional velocity profiles are almost similar for different values of offset ratio. It is due to the fact that offset jet flow attains the characteristics of a wall jet type flow in the wall jet region.

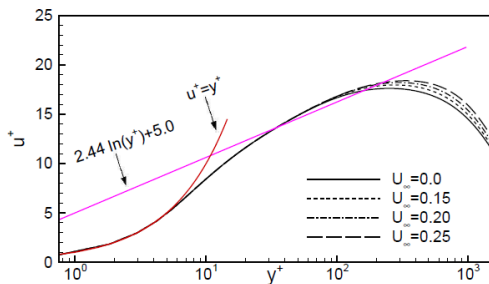


Fig. 7. Variation of non-dimensional profile ($u^+ = y^+$) with different values of freestream velocity for $Re=15000$ and $OR=7$.

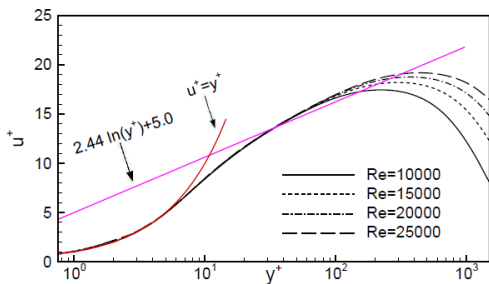


Fig. 8. Variation of non-dimensional profile ($u^+ = y^+$) with different values of Reynolds number for $OR=7$ and $U_{inf} = 0.2$.

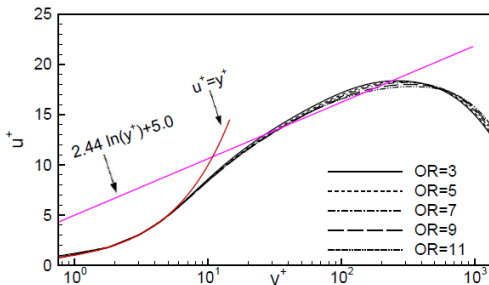


Fig. 9. Variation of non-dimensional profile ($u^+ = y^+$) with different values of offset ratio for $OR=7$ and $Re=15000$.

4.1 Solid-Fluid Interface Temperature

Figure 10 illustrates the axial variation of solid-fluid interface temperature for different values of thermal

conductivity ratio (K) for $OR = 7$, $Re = 15000$, $S = 15$, $U_\infty = 0.20$. The interface temperature (θ_i) decreases in the recirculation region due to presence of primary recirculation region which is responsible for better mixing and transport of heat away from the surface. The interface temperature is minimum at the reattachment point due to impingement of jet on the surface. The jet attaches with the solid surface at the reattachment point thereafter impingement region starts. The interconversion of pressure into velocity takes place in the impingement region. The interface temperature increases in the wall jet region due to decrease in heat transfer rate along the axial direction. The heat transfer rate decreases as the boundary layer thickness grows in the axial direction with corresponding decay in velocity near the wall. At a given axial position, interface temperature is higher for higher value of thermal conductivity ratio which allows heat transfer to take place at an enhanced rate.

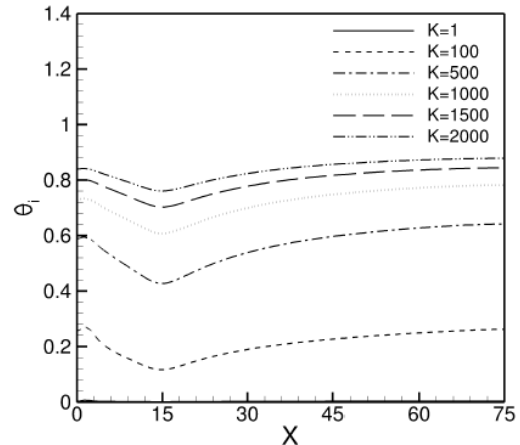


Fig. 10. Variation of interface temperature for different values of thermal conductivity ratio (K) for $OR = 7$, $Re = 15000$, $S = 15$, $U_\infty = 0.20$.

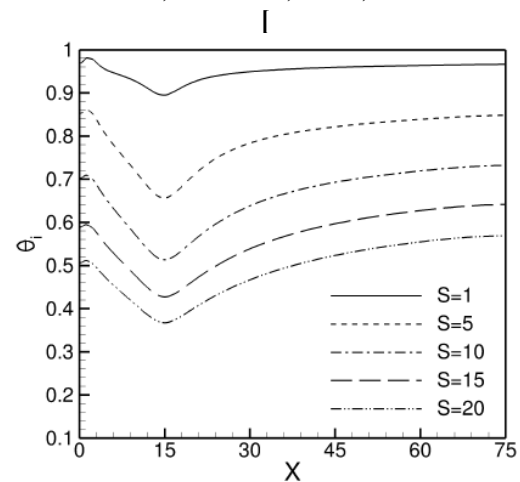


Fig. 11. Variation of interface temperature for different S for $Re = 15000$, $k = 500$, $OR = 7$, $U_\infty = 0.20$.

Figure 11 shows the axial variation of interface temperature for different values of non-dimensional

plate thickness (S) where other parameters are taken as $Re = 15000$, $K = 500$, $OR = 7$ and $U_\infty = 0.20$. The interface temperature is higher for lower value of plate thickness. The resistance to conduction heat transfer within the solid plate increases with increase in thickness of solid plate. Thus, interface temperature decreases with increase in thickness of solid plate. The local maxima close to the jet inlet is due to the presence of secondary recirculation region. The effect of Reynolds number on the variation of interface temperature along the axial direction is illustrated in Fig. 12 for $OR = 7$, $K = 500$, $S = 15$ and $U_\infty = 0.20$. The higher Reynolds number contributes toward better cooling reflected by decrease in the interface temperature with increase in Reynolds number. The interface temperature just downstream of jet exit increases due to the presence of secondary recirculation regions (Moffatt vortices). The momentum of fluid in the secondary recirculation regions is less compared to the primary recirculation region.

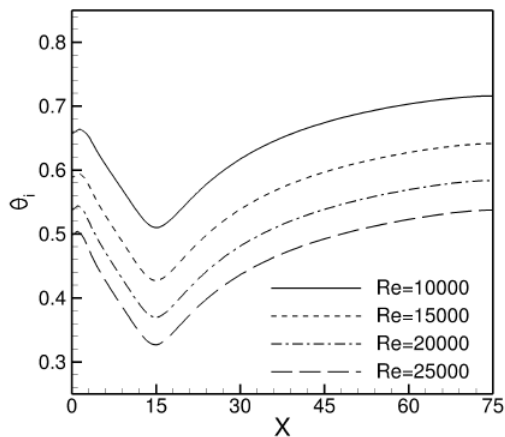


Fig. 12. Variation of interface temperature for different Reynolds number (Re) for $OR = 7$, $k = 500$, $S = 15$, $U_\infty = 0.20$.

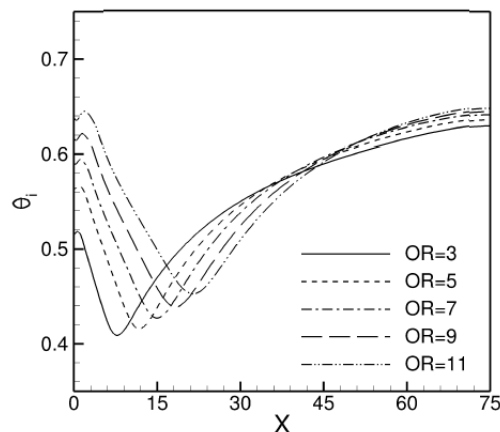


Fig. 13. Variation of interface temperature for different offset ratios for $Re = 15000$, $k = 500$, $S = 15$, $U_\infty = 0.20$.

The dependence of interface temperature on offset ratio is illustrated in Fig. 13 by keeping the other

parameters constant as $Re = 15000$, $K = 500$, $S = 15$ and $U_\infty = 0.20$. The interface temperature is lower in the recirculation region for offset jet with lower offset ratio. This is due to the fact that the size of primary recirculation region increases with increase in offset ratio. A bigger recirculation region implies that it requires more energy for sustaining its motion from mean flow. For same Reynolds number at the jet inlet, offset jet with lower offset ratio has more potential for cooling the heated surface. Thus, cooling effectiveness of offset jet decreases with increase in offset ratio. Figure 14 shows the axial variation of interface temperature for different values of freestream velocity. The interface temperature decreases in the recirculation region (except very close to the nozzle exit) due to mixing induced by the primary recirculation region. The variation of interface temperature very close to the wall can be attributed to the presence of secondary recirculation region. The interface temperature is lower in the recirculation region in case of quiescent medium and increases with increase in freestream velocity. This is due to decrease in the entrainment of surrounding fluid with increase in freestream velocity. The variation of interface temperature in the wall jet region with freestream velocity is very small as observed in Fig. 14.

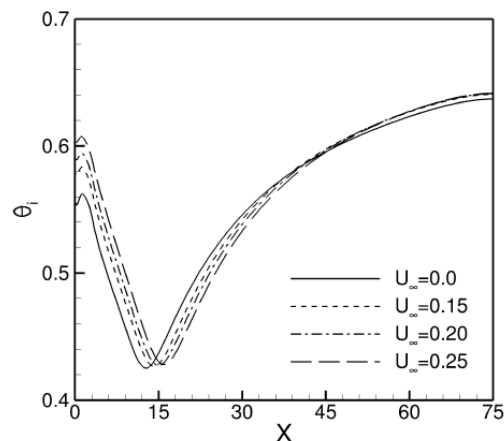


Fig. 14. Variation of interface temperature for different U_∞ for $Re = 15000$; $OR = 7$; $K = 500.0$; $S = 15$.

4.2 Local Nusselt Number Variation at Solid-Fluid Interface

The axial variation of local Nusselt number along the plate is shown in Fig. 15 for different values of solid to fluid thermal conductivity ratio (K) i.e. $K = 1, 100, 500, 1000, 1500, 2000$. The other parameters are taken as $OR = 7$, $Re = 15000$, $S = 15$ and $U_\infty = 0.20$. The local Nusselt number increases with downstream distance inside the recirculation region and attains the peak value at the reattachment point. The rotation of fluid in the primary recirculation region causes better mixing. The decrease in the local Nusselt number just downstream of the jet inlet is due to existence of the secondary recirculation regions.

The local Nusselt number decreases in the impingement region and the wall jet region with downstream distance. The effect of thermal conductivity ratio on the local Nusselt number is very small as observed in Fig. 15. Figure 16 illustrates the effect of non-dimensional plate thickness (S) on the axial variation of local Nusselt number at the solid-liquid interface. The other parameters are taken as $OR = 7$, $Re = 15000$, $K = 500$ and $U_\infty = 0.20$. It has been observed that local Nusselt number is nearly independent of plate thickness (S). Thus, based on observations made in Figs. 15 and 16, local Nusselt number is not much influenced by solid properties. The Nusselt number is mainly influenced by flow conditions and fluid properties. The effect of Reynolds number on axial variation of local Nusselt number for $OR = 7$, $K = 500$, $S = 15$ and $U_\infty = 0.20$ is shown in Fig. 17. The local Nusselt number is higher for higher Reynolds number as expected. Also, the axial location of peak Nusselt number is independent of Reynolds number of the jet. The effect of various offset ratios on the axial variation of local Nusselt number for $Re = 15000$, $K = 500$, $S = 15$ and $U_\infty = 0.20$ is shown in Fig. 18 at the solid-fluid interface. The peak value of Nusselt number decreases with increase in offset ratio of the jet. This is due to the fact that size of recirculation region increases with increase in offset ratio. The offset jet interacts with the rotating fluid of primary recirculation region. Thus, for same Reynolds number at the jet inlet, the decay in momentum of the offset jet is higher for larger recirculation region due to momentum exchange. The effect of freestream velocity (U_∞) on axial variation of Nusselt number is shown in Fig. 19 for $Re = 15000$, $OR = 7$, $K = 500$ and $S = 15$ at the solid-fluid interface. The local Nusselt number in the primary recirculation region decreases with increase in freestream velocity. The entrainment of surrounding fluid into the offset jet is more in case of quiescent medium i.e. when freestream velocity is zero and it decreases with increase in freestream velocity.

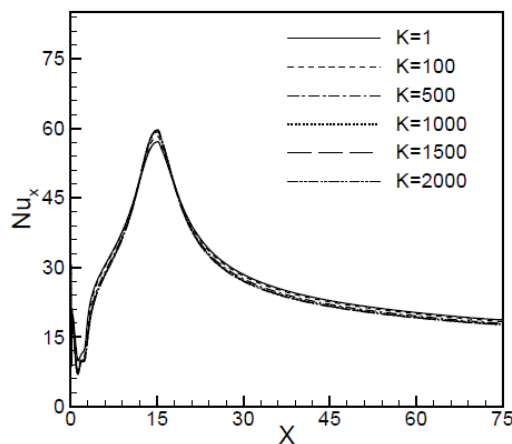


Fig. 15. Variation of Nusselt number for different values of thermal conductivity (k) for $OR = 7$, $Re = 15000$, $S = 15$, $U_\infty = 0.20$.

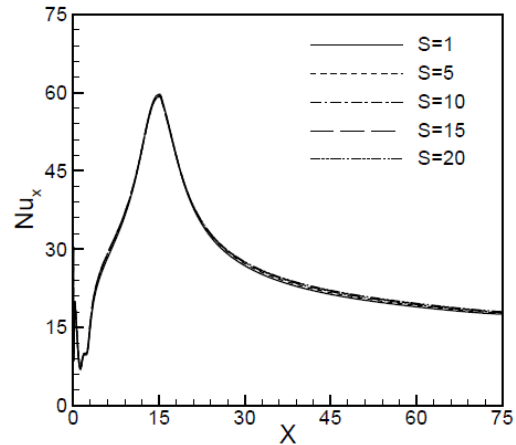


Fig. 16. Variation of Nusselt number for different S for $Re = 15000$, $k = 500$, $OR = 7$, $U_\infty = 0.20$.

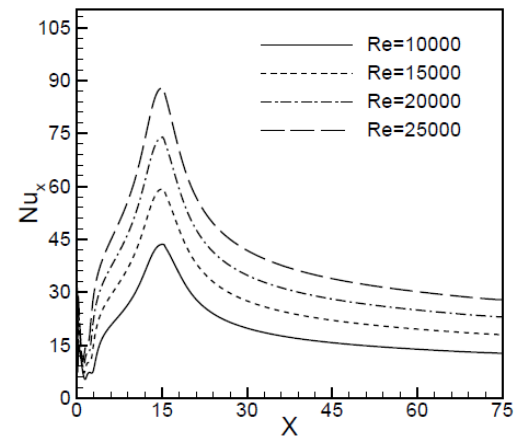


Fig. 17. Variation of Nusselt number for different Reynolds number (Re) for $OR = 7$, $k = 500$, $S = 15$, $U_\infty = 0.20$.

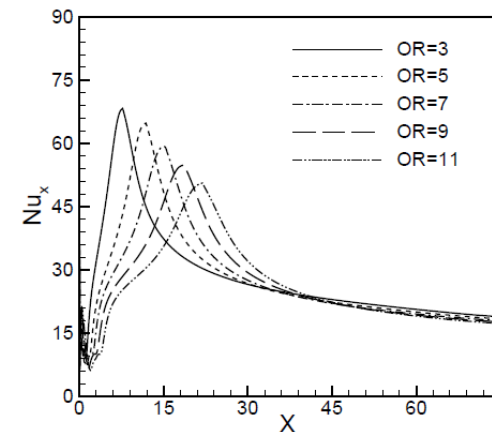


Fig. 18. Variation of Nusselt number for different offset ratios for $Re = 15000$, $k = 500$, $S = 15$, $U_\infty = 0.20$.

Since the freestream moves in the same direction as that of the jet, the resisting shear stress acting at the outer edge of the jet is higher in case of quiescent medium and decreases with increase in freestream velocity. For the range of freestream velocity

considered, the effect of freestream velocity on the axial variation of Nusselt number is very small in the wall jet region as shown in Fig. 19.

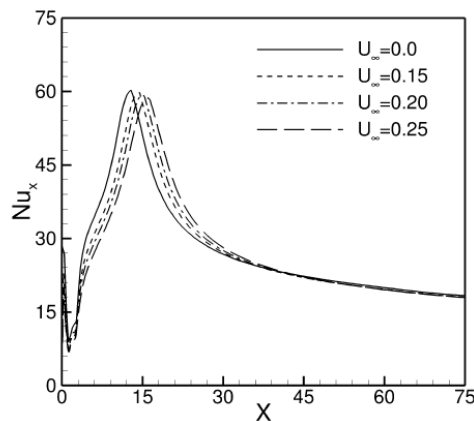


Fig. 19. Variation of Nusselt number for different U_∞ for $Re = 15000$; $OR = 7$; $K = 500.0$; $S = 15$.

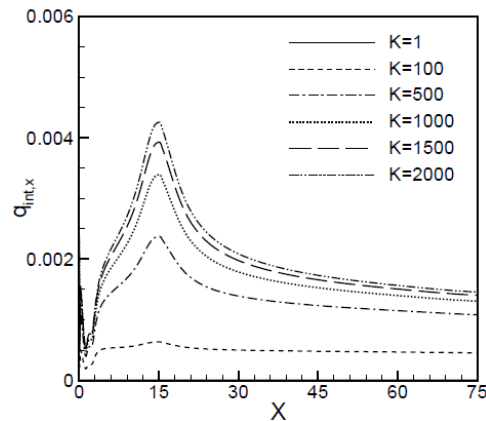


Fig. 20. Variation of heat flux at interface for different values of thermal conductivity (k) for $OR = 7$, $Re = 15000$, $S = 15$, $U_\infty = 0.20$.

4.3 Heat Flux Variation at Solid-Fluid Interface

Figure 20 shows the effect of solid to fluid thermal conductivity ratio on axial variation of local heat flux along solid-fluid interface for $OR = 7$, $Re = 15000$, $S = 15$, $U_\infty = 0.20$. The local heat flux at the interface increases with increase in solid to fluid thermal conductivity ratio K . The higher thermal conductivity of solid offers lower resistance to heat transfer. The variation of plate thickness (S) and its effect on local heat flux along the solid-fluid interface is shown in Fig. 21 for $Re = 15000$, $K = 500$, $OR = 7$ and $U_\infty = 0.20$. The local heat flux is higher for lower value of S as the resistance to heat transfer increases with increase in thickness of plate. The effect of offset ratio of jet on the local heat flux along the interface is shown in Fig. 22 for $Re = 15000$, $K = 500$, $S = 15$ and $U_\infty = 0.20$. The peak value of local heat flux is observed for $OR = 3$ and decreases with increase in offset ratio of the jet. The axial location of peak heat flux moves downstream with increase in offset ratio of

the jet. In the wall jet region, local heat flux is higher for lower offset ratio and decreases with increase in offset ratio. This is due to the fact that momentum of the jet in the wall jet region is higher for $OR = 3$ and reduces with increase in offset ratio. The effect of variation of Reynolds number on the axial variation of local heat flux is shown in Fig. 23 for $OR = 7$, $K = 500$, $S = 15$, $U_\infty = 0.20$. The local heat flux is higher for higher Reynolds number. The peak value of local heat flux is observed at the same axial location, as the reattachment length remains nearly same for the range of Reynolds number considered in the present problem. For sufficiently high Reynolds number ($Re > 15000$), the reattachment length becomes independent of Reynolds number as reported by Pelfrey and Liburdy (1986). Bourque and Newmann (1960) have also found the same conclusion using dimensional analysis that for large Reynolds number, reattachment length becomes independent of Reynolds number. Figure 24 shows the axial variation of local heat flux for $Re = 15000$, $OR = 7$, $K = 500$ and $S = 15$ at the solid-fluid interface. It has been observed that local heat flux in the primary recirculation region decreases with increase in freestream velocity due to reduced mixing and entrainment as discussed earlier. The peak value of local heat flux is observed for the case of quiescent medium $U_\infty = 0$ and decreases with increase in freestream velocity. The effect of freestream velocity on the local heat flux in the wall jet region is very small as shown in Fig. 24.

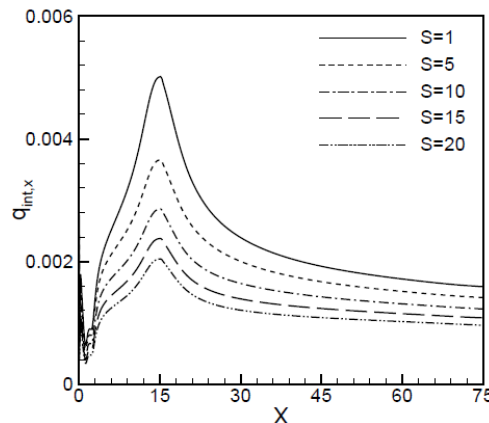


Fig. 21. Variation of heat flux at interface for different S for $Re = 15000$, $k = 500$, $OR = 7$, $U_\infty = 0.20$.

5. CONCLUSION

The present study deals with conjugate cooling of flat plate by a turbulent offset jet in the presence of freestream motion. The turbulent convection in the fluid and conduction heat transfer in the solid are solved simultaneously. The jet inlet temperature is same as that of the ambient whereas the bottom of heated flat plate is maintained at constant temperature higher than the jet inlet temperature. The effects of offset ratio of jet (OR), Reynolds number of flow (Re), solid to fluid thermal conductivity ratio (K), non-dimensional solid plate thickness (S) and freestream velocity (U_∞) on conjugate heat transfer characteristics have been investigated. The offset ratio is considered

in the range $OR = 3 - 11$, Reynolds number in the range $Re = 10000 - 25000$, solid to fluid thermal conductivity ratio in the range $K = 1 - 2000$, solid plate thickness $S = 1 - 20$ and freestream velocity in the range $U_\infty = 0.1-0.25$. For turbulence closure, low-Reynolds number $k-\omega$ SST model is considered.

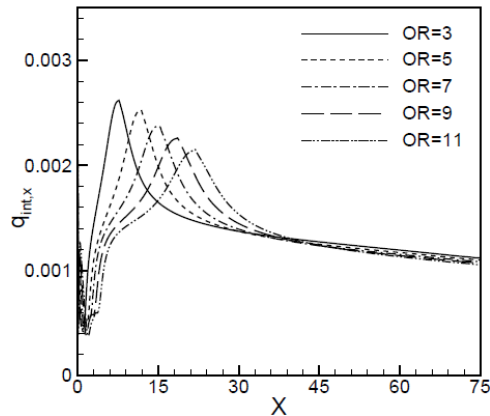


Fig. 22. Variation of heat flux at interface for different offset ratios for $Re = 15000$, $k = 500$, $S = 15$, $U_\infty = 0.20$.

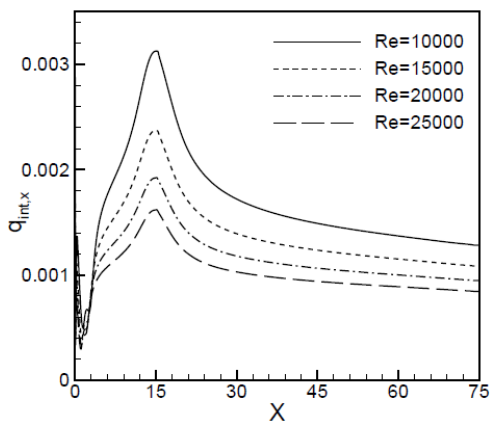


Fig. 23. Variation of heat flux at interface for different Reynolds number (Re) for $OR = 7$, $k = 500$, $S = 15$, $U_\infty = 0.20$.

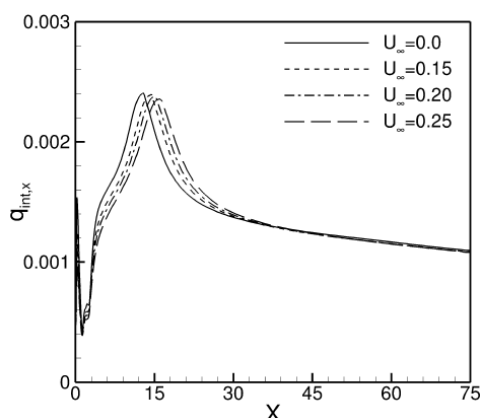


Fig. 24. Variation of heat flux at interface for different U_∞ for $Re = 15000$; $OR = 7$; $K = 500.0$; $S = 15$.

The entire boundary layer is solved including the viscous sublayer region using LRN $k-\omega$ SST

model. The presence of Moffatt vortices (secondary recirculation regions) have been identified near corner of the wall where turbulence Reynolds number is low. The size of secondary recirculation region increases with increase in offset ratio of jet. It has been found that interface temperature depends on all parameters considered i.e. Reynolds number of flow, offset ratio of jet, solid to fluid thermal conductivity ratio and solid plate thickness. The interface temperature decreases with increase in Reynolds number of flow, offset ratio of jet, solid plate thickness and increases with increase in solid to fluid thermal conductivity ratio. The interface temperature in the recirculation region increases with increase in freestream velocity. The local Nusselt number increase with increase in Reynolds number of flow but decreases with increase in offset ratio of jet. However, it is not much affected by solid property K and thickness of plate S . The local heat flux increases with decrease in value of solid plate thickness (S) and the peak value is observed at the reattachment length. The local heat flux in the primary recirculation region decreases with increase in freestream velocity due to reduced mixing and entrainment.

REFERENCES

- Ayech, S. B. H., N. M. Said, P. Bournot and G. L. Palet (2017). Investigation of a turbulent wall jet in forced convection issuing into a directed coflow stream. *Journal of Turbulence* 18(6), 539–559.
- Bardina, J. E., P. G. Huang and T. J. Coakley (1997). Turbulence modeling validation, testing and development. Technical report, NASA Technical Memorandum 110446, Ames Research Center.
- Biswas, G. and V. Eswaran (2002). *Turbulent Flows: Fundamentals, Experiments and Modeling*. IIT Kanpur Series of Advanced Texts. Narosa Publishing House, New Delhi, India.
- Bourque, C. and B. G. Newman (1960). Reattachment of two-dimensional incompressible jet to an adjacent plate. *Aeronautical Quarterly* 11, 201–232.
- Chien, K. Y. (1982). Predictions of channel and boundary layer flows with a low-Reynolds number turbulent model. *American Institute of Aeronautics and Astronautics Journal* 20, 33–38.
- Deo, R. C., G. J. Nathan and J. Mi (2007). Comparison of turbulent jets issuing from rectangular nozzles with and without sidewalls. *Experimental Thermal Fluid Sciences* 32, 596–606.
- Doormaal, J. P. V. and G. D. Raithby (1984). Enhancements of the SIMPLE method for predicting incompressible fluid flows. *Numerical Heat Transfer* 7, 147–163.
- Gao, N. and D. Ewing (2007). Experimental

- investigation of planar offset attaching jets with small offset distances. *Experiments in Fluids* 42, 941–954.
- Herrero, J., F. X. Grau, J. Grifoll and F. Giralt (1991). A near wall κ - ϵ formulation for high p randtl number heat transfer. *International Journal of Heat and Mass Transfer* 34, 711–721.
- Habli, S., N. M. Saïd, G. L. Palec and H. Bournot (2014). Numerical study of a turbulent plane jet in a coflow environment. *Computers & Fluids* 29, 20–28.
- Hoch, J. and L. M. Jiji (1981). Theoretical and experimental temperature distribution in two-dimensional turbulent jet boundary interaction. *Transaction ASME Journal of Heat Transfer* 103, 331–335.
- Hoch, J. and L. M. Jiji (1981(a)). Two-dimensional turbulent offset jet-boundary interaction. *Transaction ASME Journal of Fluid Engineering* 103, 154–161.
- Hofmann, H. M., R. Kaiser, M. Kind and H. Martin (2007). Calculations of steady and pulsating impinging jets-an assessment of 13 widely used turbulence models. *Numerical Heat Transfer, Part B: Fundamentals* 51(6), 565–583.
- Kechiche, J., H. M. hiri, G. L. Palec and P. Bournot (2004). Application of low Reynolds number κ - ϵ turbulence models to the study of turbulent wall jets. *International Journal of Thermal Sciences* 43, 201–211.
- Kim, D. S., S. H. Yoon, D. H. Lee and K. C. Kim (1996). Flow and heat transfer measurements of a wall attaching offset jet. *International Journal of Heat and Mass Transfer* 39, 2907–2913.
- Kumar, A. and M. K. Das (2011). Study of a turbulent dual jet consisting of a wall jet and an offset jet. *Transaction ASME Journal of Fluids Engineering* 133(10), 101201 (11).
- Lauder, B. E. and B. I. Sharma (1974). Application of the energy dissipation model of turbulence to the calculation of flow near a spinning disc. *Letters in Heat and Mass Transfer* 1, 131–138.
- Lauder, B. E. and W. Rodi (1981). The turbulent wall jet. *Progress in Aerospace Sciences* 19, 81–128.
- Menter, F. R. (1994). Two-equation eddy-viscosity turbulence models for engineering applications. *American Institute of Aeronautics and Astronautics Journal* 32(8), 598–1605.
- Menter, F. R. (2009). Review of the shear-stress transport turbulence model experience from an industrial perspective. *International Journal of Computational Fluid Dynamics* 23(4), 305–316.
- Menter, F. R., M. Kuntz and R. Langtry (2003). Ten years of industrial experience with the SST turbulence model. In K. Hanjalic, Y. Nagano, and M. Tummers, editors, *Turbulence, Heat and Mass Transfer 4*. Begell House, Inc.
- Moffatt, H. K. (1964). Viscous and resistive eddies near a sharp corner. *Journal of Fluid Mechanics* 18(1), 1–18.
- Mondal, T., A. Guha and M. K. Das (2016). Analysis of conjugate heat transfer for a combined turbulent wall jet and offset jet. *ASME: Journal of Heat Transfer* 138, 051701-1 to 051701-13.
- Nagano, Y. and M. Hishida (1987). Improved form of the κ - ϵ model for wall turbulent shear flows. *Transaction ASME Journal of Fluids Engineering* 109, 156–160.
- Patankar S. V. (1980). *Numerical Heat Transfer and Fluid Flow*. Hemisphere, New York.
- Pelfrey, J. R. R. and J. A. Liburdy (1986). Mean flow characteristics of a turbulent offset jet. *Transaction ASME Journal of Fluids Engineering*, 108, 82–88.
- Rathore, S. K. and M. K. Das (2015). A comparative study of heat transfer characteristics of wall-bounded jets using different turbulence models. *International Journal of Thermal Sciences*, 89, 337–356.
- Rathore, S. K. and M. K. Das (2016). Effect of freestream motion on heat transfer characteristics of turbulent offset jet. *ASME: Journal of Thermal Science and Engineering Applications* 8, 011021-1 to 011021-12.
- Shuja, S. Z., B. S. Yilbas and M. O. Budair (1999). Gas jet impingement on a surface having a limited constant heat flux area: Various turbulence models. *Numerical Heat Transfer: Part A* 36(2), 171–200.
- Tritton, D. J. (1977). *Physical Fluid Dynamics*, Von Norstrand Reinhold, UK.
- Versteeg, H. K. and W. Malalasekera (1996). *An Introduction to Computational Fluid Dynamics. The Finite Volume Method*. Addison Wesley Longman Limited, England, ISBN 1-582-21884-5.
- Vishnuvardhanarao, E. and M. K. Das (2007). Study of conjugate heat transfer from a flat plate by turbulent offset jet flow. *Numerical Heat Transfer, Part A: Applications* 53(5), 524–542.
- Vishnuvardhanarao, E. and M. K. Das (2009). Conjugate heat transfer study of incompressible turbulent offset jet flows. *Heat and Mass Transfer* 45, 1141–1152.
- Yang, Z. and T. H. Shih (1993). New time scale based κ - ϵ model for near-wall turbulence. *American Institute of Aeronautics and Astronautics Journal* 31(7), 1191–1198.

